nature energy

SUPPLEMENTARY INFORMATION

https://doi.org/10.1038/s41560-018-0237-6

In the format provided by the authors and unedited.

Langmuir–Blodgett artificial solid-electrolyte interphases for practical lithium metal batteries

Mun Sek Kim[1], Ji-Hyun Ryu[1,2], Deepika[3], Young Rok Lim[1,4], In Wook Nah[1], Kwang-Ryeol Lee[3], Lynden A. Archer[5]* and Won Il Cho[1]*

[1]Center for Energy Storage Research, Korea Institute of Science and Technology, Seoul, Republic of Korea. [2]Department of Materials Science and Engineering, Korea University, Seoul, Republic of Korea. [3]Center for Computational Science Research, Korea Institute of Science and Technology, Seoul, Republic of Korea. [4]Department of Chemistry, Korea University, Sejong, Republic of Korea. [5]School of Chemical and Biomolecular Engineering, Cornell University, Ithaca, NY, USA. *e-mail: laa25@cornell.edu; wonic@kist.re.kr

Supplementary Note 1. Analysis on the nucleation overpotential voltage profiles

The voltage profiles provide three essential facts about Li migration processes: Coulombic trade-off of a system, mass-transfer controlled potential and nucleation overpotential. The Coulombic trade-off reports utilization of charges, which can be attributed to electrochemical reactions involved in a system and formation of intrinsic SEIs on electrodes' interfaces. The mass-transfer controlled potential represents a steady-state process of the Li migration; this potential is therefore strongly dependent on applied current densities, migrating substrates and electrolytes. The nucleation overpotentials can quantitatively represent a degree of which the Li atoms nucleate and grow on migrating substrates. Hence, the overpotential provides a size of energy barriers that must be scaled to form Li nuclei[1,2] on defined substrates, and the substrates with strong interaction of the Li and good conductivity should have therefore the low nucleation overpotentials and the small mass-transfer controlled potentials.

Supplementary Note 2. Optimization of the LBASEI thickness

From the definition, μ_{nuc} would be expected to vary with thicknesses of the LBASEI. As the thickness increases in Fig. 3c, μ_{tip} decreases steeply up to the thickness of approximately 2 μm, and μ_{mtc} slightly increases due to the increase of a Li diffusion volume of the LBASEI. Additionally, the transient potential (μ_{tr}), the potential that starts to achieve a steady-state Li migration potential and lies between μ_{tip} and μ_{mtc}, increases with respect to the increasing the thickness. As the thickness of the LBASEI increases, μ_{tip} is reduced due to the increased number of favourable nucleation sites that are available within the total volume of the LBASEI, and μ_{mtc} is increased slightly as higher potential is needed to deposit the Li all of interlayer gaps and under/above[3] the LBASEI. This also causes μ_{tr} to shift as more time, with the fixed galvanostatic current of 0.05 mA cm^{-2}, is required for reaching steady migration states of the Li in the LBASEI based on the different total volume available for the Li migration process. Importantly, the μ_{nuc} tends to remain steady for the LBASEI thicknesses above ~2 μm, providing a convenient approach for optimizing the thickness for the LBASEI at the given conditions. The steady μ_{nuc} trend is achieved above the certain thickness as the amount of migrant Li, which is defined by the applied current density and time, is balanced and optimized with the number of favourable interactive sites of the Li present in the LBASEI. This is in turn proportional to the total volume or thickness of the LBASEI. Although the μ_{nuc} may vary with a degree of the applied current densities, large deviation of μ_{nuc} trend is expected for the high current densities as the higher degree of perturbations of the Li nucleation/growth is introduced. Therefore, relatively low current is desired to precisely analyse the μ_{nuc} trend and for the thickness optimizations.

Supplementary Note 3. Interfacial impedance analysis on the LBASEI Li and pristine Li

The reduced impedance of the LBASEI Li anode is due to a favoured Li interaction *via* available functional groups, highly conducting surface features of the LBASEI and protection of the LiM surface with the LBASEI to a reactive environment. The interfacial impedance of the LBASEI Li anode increased whereas the pristine Li anode is decreased after cycling. This can be explained by the behaviour of a SEI evolution and a Li deposition process. As a smooth deposition of the Li occurs at the LBASEI Li anode, slightly increased surface impedance is expected due to formation of intrinsic SEIs at the LBASEI and the growing Li interfaces. Whereas the decrease of the impedance is expected for the cycled pristine Li anode as unstable nucleation of the Li induces rougher electrodeposits of the Li and breakage of native oxide and passivation layers on the pristine Li anode, which ultimately increases the surface area of the anode and expose the

fresh Li to the reactive liquid electrolyte[3]. It is important to note that the few cycled cells are used to observe the interfacial impedances to relate the evolution of surface characteristics from the initial condition; investigating large number cycled cells may limitedly exhibit only the magnitude of the increased interfacial impedance, not a broader spectrum of the interfacial evolution from the beginning.

Supplementary Note 4. Charge-discharge voltage profile analysis

The cycle life of the LiMBs is mainly restricted by high interfacial impedances, at given C rates, of the anode caused by piling up of orphaned Li dendrites and insulating SEIs that grow over cycles[4], and degradation of cathode electrolyte interphases (CEIs) and electrolytes working at high potentials for intercalation cathodes[5] also significantly, but not as much as for the LiM anode, restricts prolonged cycle life of the LiMBs. Therefore, observing the voltage profiles, especially for the charging, is essential to understand evolutions of the electrode conditions in cells. Fig. 6b shows the voltage profiles of the pristine Li|NCM cell with E-2 electrolyte for 1^{st}, 100^{th}, 200^{th}, 300^{th} and 400^{th} cycles. At the 1^{st} charging voltage profile, there is the potential spike, marked by the dashed red circle in Fig. 6b, that indicates unstable electrochemical activation of the cell. Note that no formation cycle is performed on the cell in purpose to observe the performance variations between the reference (pristine Li|NCM) and modified (PrGO Li|NCM) cells more evidently. Furthermore, the interfacial impedance evolution can be observed by tracing the intersection between the charging and discharging voltage profiles at the specified cycles. When the intersections are traced in Fig. 6b, the intersection points gradually move leftward and up as the cycle number increases. The intersection points moving horizontally leftward indicates there is a limited utilization of active materials at the given C rate, which could be induced by the structural and CEI degradation of the cathode, and the intersection points moving up means there is a gradual increase of the interfacial impedance for the anode that cannot operate normally with respect to previous cycles at the given C rate. Hence, the direction of the traced intersection points, moving leftward and up, reveals the reasons why the cell failure occurred, which is due to surface and structural destruction of the anode and cathode. Fig. 6c shows the voltage profiles of the PrGO Li|NCM cell with E-2 electrolyte for 1^{st}, 100^{th}, 200^{th}, 300^{th} and 400^{th} cycles. Compared with Fig. 6b, the much lesser potential spike at the beginning of the charging voltage profile is observed. This means that the LBASEI Li anode is able to stably allow electrochemical reaction at 1C without the need of the formation cycle, which also agrees with the interfacial impedance result in Fig. 4d. Furthermore, the trace of the intersection points only moves horizontally leftward. This voltage profile evolution indicates that the anode is reversibly and stably migrating the Li between the LBASEI Li and NCM electrodes without restricting the cell performance by the means of electrodes' high interfacial impedances.

Supplementary Note 5. Cyclic voltammogram analysis

To further clarify the redox reactions occurring in the full cells, cyclic voltammetry is performed for the pristine Li|NCM and the LBASEI Li|NCM cells with the scanning voltage window of 3-4.2 V and at the scan rate of 0.01 mV s^{-1}. Cyclic voltammograms of the first 11 cycles are shown in Fig. 6h for the pristine Li|NCM cell. There are noticeable redox peak shifts, indicated by the dashed red arrows, from 1^{st} to 2^{nd} cycle, indicating the unstable electrochemical activation at the 1^{st} cycle. This result is in agreement with the 1^{st} cycle voltage profile in Fig. 6b where the potential spike appeared at the beginning of the 1^{st} charging process. Also, the anodic peaks slowly diverge as cycle number increases; this is caused by the formation of the Li dendrites and

pile up of insulating SEIs at the LiM anode interface that cause additional reactions, which mostly happens during the charging processes. However, cyclic voltammograms for the LBASEI Li|NCM cell exhibit stable redox reactions for both anodic and cathodic sweeps (Fig. 6i). Despite having anodic scan peak shifts due to the activation, indicated after the 1st and 2nd anodic sweeps with the dashed red arrow, lesser peak shifts at the beginning of the anodic sweep are observed, and also stable redox reactions occur reversibly during the cycles as shown in Fig. 6i. Therefore, above results indicate that the LBASEI stabilize the Li migration electrochemically in the full cells.

Supplementary Note 6. Electrochemical effect of the n/p ratios

The CE associated with the first cycle may vary with the total amount of the migrant Li, which is defined by the cathode loading (in this case the 4.1 mAh cm^{-2} for the cathode capacity, which theoretically passes 19.89 μm thick LiM assuming a flat deposition). The reasoning is briefly summarized as follows. For a low loading cathode, relatively higher portions of freshly deposited Li will be consumed to form intrinsic SEIs than that of a high loading cathode due to differences in the total amount of the migrant Li with relatively steady consumption rate of the Li for the SEI formations (See Fig. 6a and 6d & Supplementary Fig. 11)[6]. Since the equal capacity cathodes are used for Fig. 7a-c, the CE may weakly be affected by the change in the n/p ratios (Fig. 6a and 6d & Supplementary Fig. 11). The capacity, on the other hand, may vary with the change in the n/p ratios as the Li utilization per cycle depends on the anodes' morphologies, intrinsic SEIs and degradation layers, which are strong function of the charging current densities. High charging current density usually induces expedited corrosion process to the LiM anode, and it has been reported that there are different thicknesses of the degradation layers forming at the anodes' interfaces with respect to the charging C rates, yielding thicker Li degradation layers with higher charging current densities[6]. Thus, mild or low charging C rate is desired for utilizing the thin LiM anode for LiMBs. Accordingly, higher capacity then can be possibly obtained with thicker Li due to better Li utilization for the anode with the presence of the degradation layers, where the effect can be seen in Fig. 7a-c.

Supplementary Figures

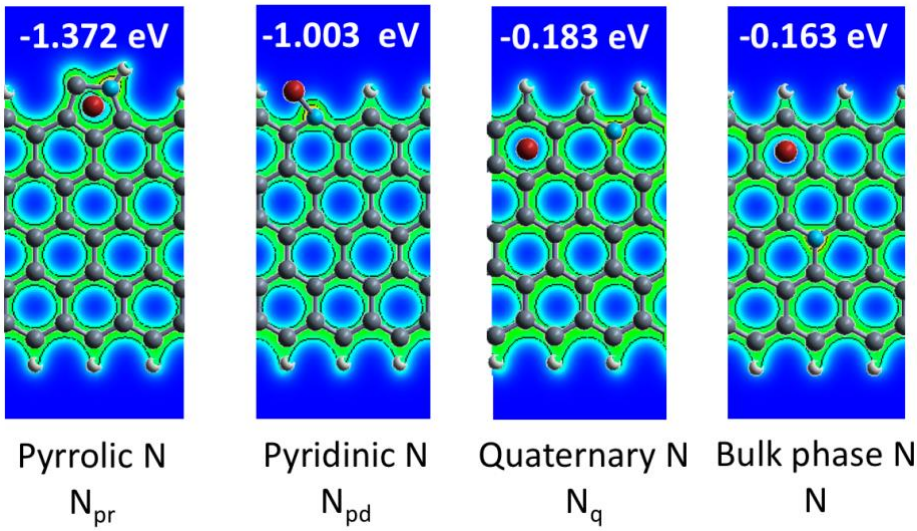

Supplementary Fig. 1 | Projected charge density after the Li atom adsorption on N_{pr}, N_{pd}, N_q and N. The charge density is plotted along (001) plane. Grey, white, maroon, red and emerald spheres represent carbon, hydrogen, lithium, oxygen and nitrogen atoms, respectively. The red region corresponds to higher charge density in reference to the blue region.

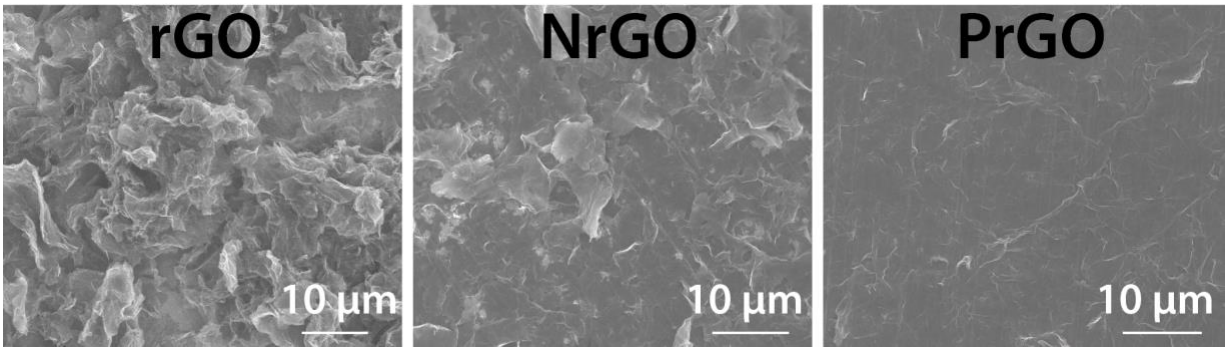

Supplementary Fig. 2 | Morphologies of rGO, NrGO and PrGO LBASEIs on Cu. rGO, NrGO and PrGO LBASEIs are fabricated *via* LBS method, and corresponding morphologies of the LBASEIs are shown.

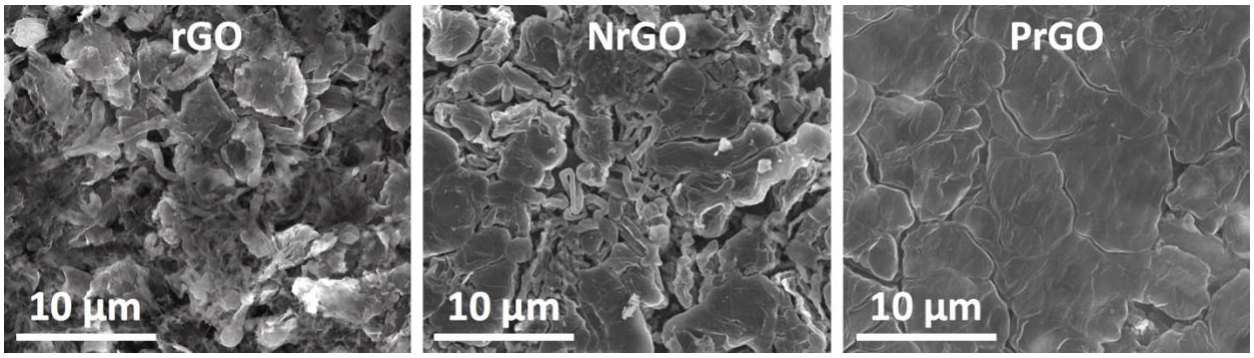

Supplementary Fig. 3 | Morphologies of Li electrodeposits on rGO, NrGO and PrGO LBASEIs. The applied current density and capacity are 0.05 mA cm^{-2} and 0.5 mAh cm^{-2} with E-3 electrolyte.

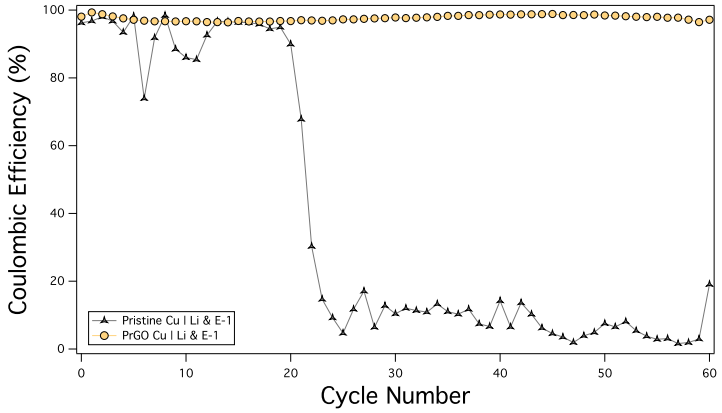

Supplementary Fig. 4 | Coulombic efficiency measurements for the LBASEI Li and the pristine Li asymmetric cells. The applied current density and capacity are 3 mA cm^{-2} and 3 mAh cm^{-2} with E-1 electrolyte.

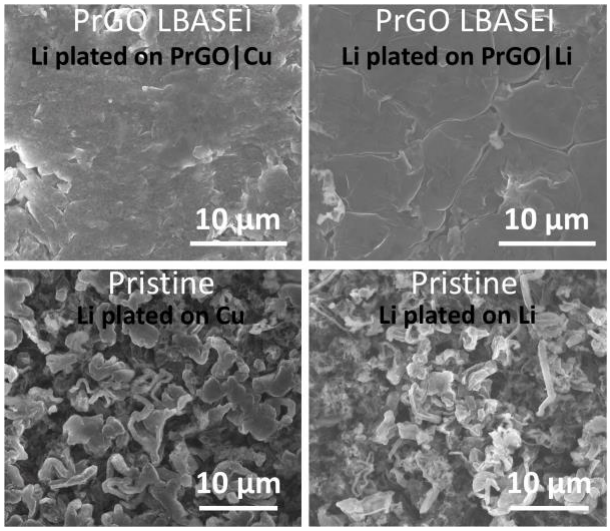

Supplementary Fig. 5 | Li electrodeposits on the asymmetric cell electrodes. SEM images of 1 mAh cm^{-2} Li deposited on the LBASEI Cu (Top left), the LBASEI Li (Top right), the pristine Cu (Bottom left) and the pristine Li (Bottom right) with E-1 electrolyte.

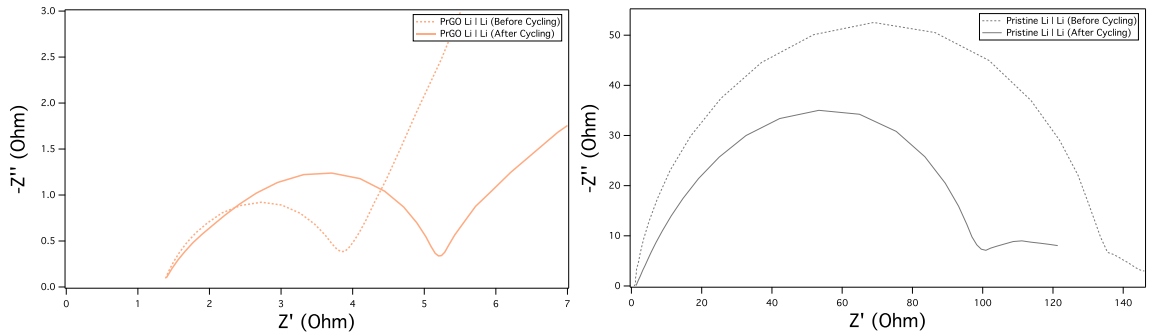

Supplementary Fig. 6 | Nyquist plots of symmetric cells for before and after cycle. Nyquist plots for the LBASEI Li and the pristine Li symmetric cells before and after 10th cycle with E-1 electrolyte.

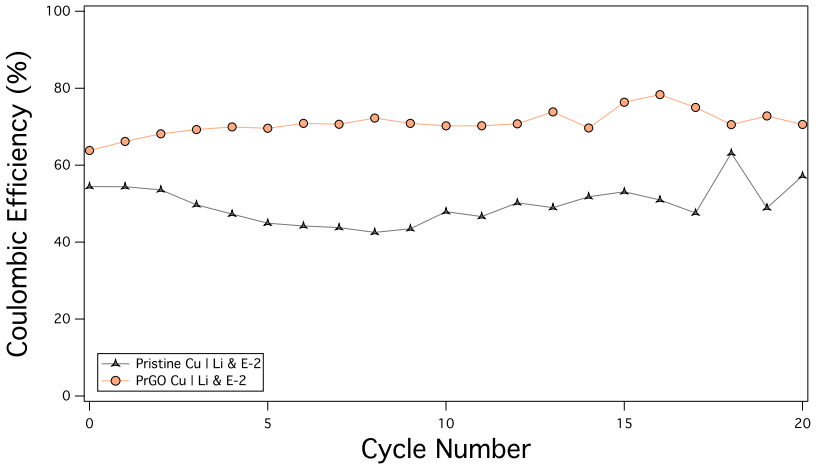

Supplementary Fig. 7 | Coulombic efficiencies of the LBASEI Li and the pristine Li asymmetric cells. Coulombic efficiency measurements of the LBASEI Li and the pristine Li asymmetric cells at the current density and capacity of 1 mA cm^{-2} and 1 mAh cm^{-2} with E-2 electrolyte.

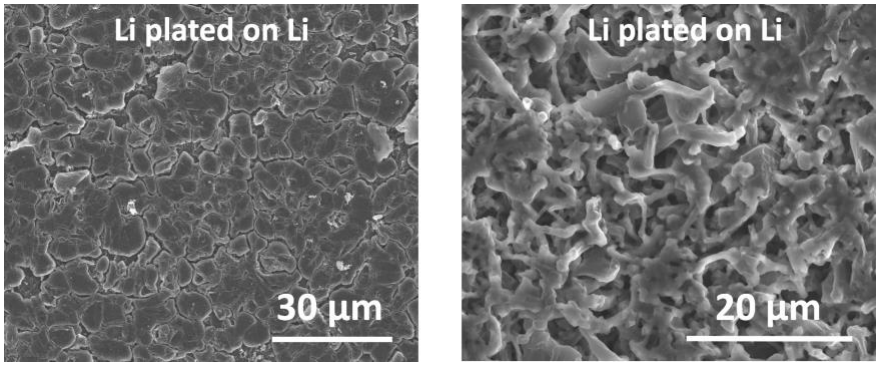

Supplementary Fig. 8 | Electrodeposited Li on the LBASEI Li and the pristine Li. SEM images of 1 mAh cm^{-2} Li deposited on the LBASEI Li (left) and the pristine Li (right) with E-2 electrolyte.

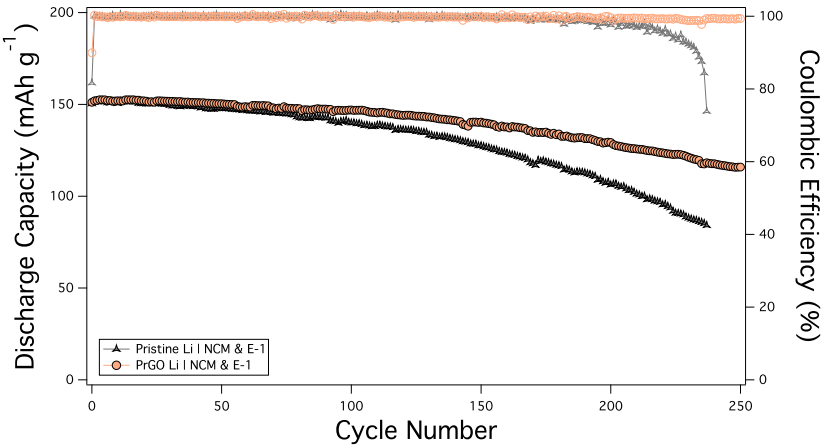

Supplementary Fig. 9 | Cycling performance of the LBASEI Li anode in the full cell. Cycling profiles for the LBASEI Li anode with NCM cathode at charging/discharging rates of 1C (1.9 mA cm^{-2}) with E-1 electrolyte.

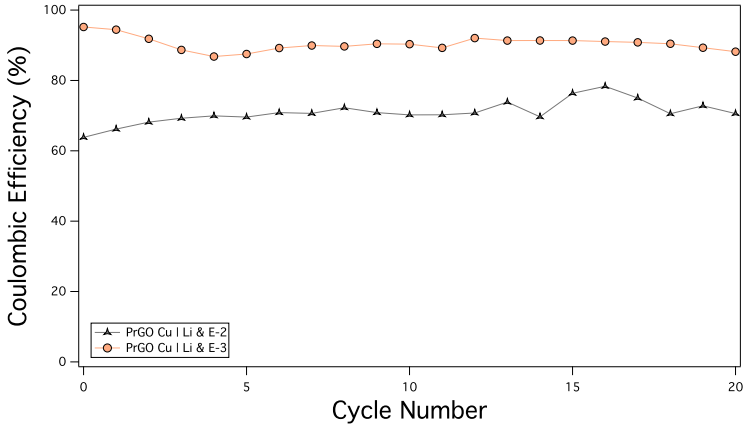

Supplementary Fig. 10 | Coulombic efficiency of the LBASEI Li asymmetric cells with different electrolytes. Coulombic efficiency measurements of the LBASEI Li asymmetric cells at the current density and capacity of 1 mA cm^{-2} and 1 mAh cm^{-2} with E-2 and E-3 electrolytes.

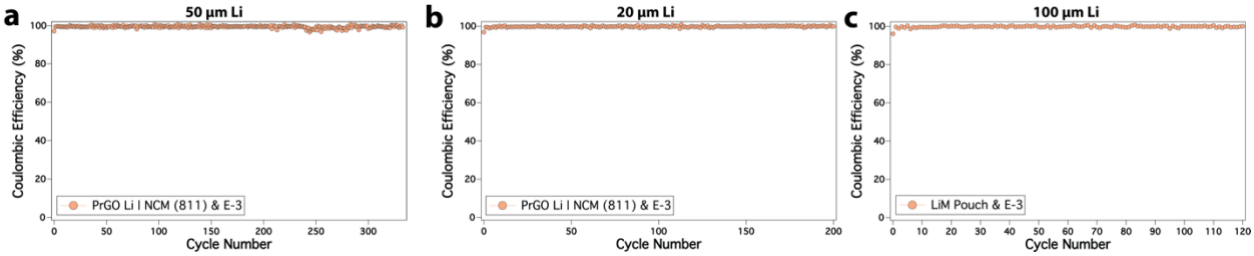

Supplementary Fig. 11 | Cycling Coulombic efficiencies of Fig. 7a-c. a, Corresponding, Fig. 7a, Coulombic efficiencies of the LBASEI on 50 µm Li with NCM(811) cell. **b**, Corresponding, Fig. 7b, Coulombic efficiencies of the LBASEI on 20 µm Li with NCM(811) cell. **c**, Corresponding, Fig. 7c, Coulombic efficiencies of the LBASEI on 100 µm Li with NCM(811) pouch battery.

Supplementary References

1. Yan, K. *et al.* Selective deposition and stable encapsulation of lithium through heterogeneous seeded growth. *Nat. Energy* **1,** 16010 (2016).

2. Zhang, R. *et al.* Lithiophilic Sites in Doped Graphene Guide Uniform Lithium Nucleation for Dendrite-Free Lithium Metal Anodes. *Angew. Chemie - Int. Ed.* **56,** 7764–7768 (2017).

3. Lin, D. *et al.* Layered reduced graphene oxide with nanoscale interlayer gaps as a stable host for lithium metal anodes. *Nat. Nanotechnol.* **11,** 626–632 (2016).

4. Cheng, X. B., Zhang, R., Zhao, C. Z. & Zhang, Q. Toward Safe Lithium Metal Anode in Rechargeable Batteries: A Review. *Chem. Rev.* **117,** 10403–10473 (2017).

5. Fan, X. *et al.* Non-flammable electrolyte enables Li-metal batteries with aggressive cathode chemistries. *Nat. Nanotechnol.* **13,** 715–722 (2018).

6. Jiao, S. *et al.* Behavior of Lithium Metal Anodes under Various Capacity Utilization and High Current Density in Lithium Metal Batteries. *Joule* **2,** 110–124 (2018).